frontiers | Frontiers in Electronic Materials

TYPE Original Research
PUBLISHED 24 October 2023
DOI 10.3389/femat.2023.1257490

OPEN ACCESS

EDITED BY
Ctirad Uher,
University of Michigan, United States

REVIEWED BY
Liangzi Deng,
University of Houston, United States
John Tranquada,
Brookhaven National Laboratory (DOE), United States
Minghu Fang,
Zhejiang University, China

*CORRESPONDENCE
Stephen D. Wilson,
stephendwilson@ucsb.edu

RECEIVED 12 July 2023
ACCEPTED 04 October 2023
PUBLISHED 24 October 2023

CITATION
Capa Salinas AN, Ortiz BR, Bales C, Frassineti J, Mitrović VF and Wilson SD (2023), Electron-hole asymmetry in the phase diagram of carrier-tuned CsV_3Sb_5. *Front. Electron. Mater.* 3:1257490. doi: 10.3389/femat.2023.1257490

Electron-hole asymmetry in the phase diagram of carrier-tuned CsV_3Sb_5

Andrea N. Capa Salinas[1], Brenden R. Ortiz[2], Calvin Bales[3], Jonathan Frassineti[3], Vesna F. Mitrović[3] and Stephen D. Wilson[1]*

[1]Materials Department, University of California Santa Barbara, Santa Barbara, CA, United States, [2]Materials Science and Technology Division, Oak Ridge National Laboratory, Oak Ridge, TN, United States, [3]Physics Department, Brown University, Providence, RI, United States

In this work, we study the effect of electron doping on the kagome superconductor CsV_3Sb_5. Single crystals and powders of $CsV_3Sb_{5-x}Te_x$ are synthesized and characterized via magnetic susceptibility, nuclear quadrupole resonance, and x-ray diffraction measurements, where we observe a slight suppression of the charge density wave transition temperature and superconducting temperature with the introduction of electron dopants. In contrast to hole doping, both transitions survive relatively unperturbed up to the solubility limit of Te within the lattice. A comparison is presented between the electronic phase diagrams of electron- and hole-tuned CsV_3Sb_5.

KEYWORDS

charge density waves, superconductivity, kagome lattice, carrier doping, topological metal

1 Introduction

The interplay between charge density wave (CDW) order and superconductivity (SC) in the AV_3Sb_5 (A = K, Rb, and Cs) class of kagome superconductors remains a focus of ongoing research (Ortiz et al. (2020, 2021); Yin et al., 2021). The band structure of AV_3Sb_5 hosts a series of saddle points near the Fermi level (Ortiz et al., 2019), giving rise to Van Hove singularities theorized to promote the formation of unconventional electronic states (Kang et al., 2022; Hu et al., 2022; Wang et al., 2013; Kiesel et al., 2013). At high temperatures, nesting effects combined with electron–phonon coupling are proposed to stabilize the formation of a CDW state (Tan et al., 2021; Li et al., 2021; Xie et al., 2022). At lower temperatures, superconductivity arises from this CDW state, and the coupling between the two phase transitions can provide insights into several proposed instabilities in this class of materials.

Specifically, the coupling between CDW order and SC in AV_3Sb_5 compounds has been experimentally explored through several approaches. These include tracking the evolution of both order parameters as the system is perturbed *via* chemical pressure (Ortiz et al., 2023; Li et al., 2022; Liu et al., 2022a,b; Zhou et al., 2023), change in dimensionality (Song et al., 2021; Wang et al., 2021; Song et al., 2023), external pressure (Wang et al., 2021; Feng et al., 2023; Yu et al., 2021; Chen et al., 2021; Du et al., 2021; Zhang et al., 2021; Chen et al., 2021; Zhu et al., 2022; Wang et al., 2021; Du et al., 2022; Yu et al., 2022; Zheng et al., 2022), uniaxial strain (Qian et al., 2021), and chemical doping (Oey et al., 2022a; Oey et al., 2022b; Liu Y. et al., 2022; Yang et al., 2022; Liu et al., 2023; Ding et al., 2022; Sur et al., 2023). One function of these perturbations is to shift the chemical potential about the multiple Van Hove singularities nearby; however, the dominant perturbation in the case of doping is often considered to be the orbitally selective modification of the Sb p_z pocket at the Γ point in the Brillouin zone (LaBollita and Botana, 2021).

In the case of carrier doping, hole doping has been shown to rapidly drive the suppression of long-range CDW order and an accompanying increase in the SC transition temperature (T_c) (Oey et al., 2022b; Yang et al., 2022; Oey et al., 2022a). In the case of CsV_3Sb_5, T_c evolves in a non-monotonic fashion, and two SC domes emerge. The second dome appears in the regime where the long-range CDW is fully suppressed, and there are qualitative similarities observed in the pressure-tuned phase diagram of CsV_3Sb_5 (Yu et al., 2021; Chen et al., 2021; Zhang et al., 2021). The evolution of charge correlations into an incommensurate, quasi-1D regime beyond the phase boundary of 3D CDW order suggests a link between the formation of two SC domes and a crossover in the character of charge correlations (Kautzsch et al., 2022; Feng et al., 2023).

One less explored question is whether there exists an electron-hole asymmetry in the carrier-tuned phase diagram of CsV_3Sb_5. In a rigid band shift model, the relative shift of the Van Hove points relative to E_F should be important to the response of the system, and in the more realistic case of orbitally selective doping, the impact of the relative changes in the Sb p_z mixed bands on the CDW state should inform more about their role in the formation of charge order. Prior studies have partially explored hole and electron doping via substitution on the vanadium sites of Ti (Yang et al., 2022) and Cr (Ding et al., 2022), respectively. While Ti doping shows a non-monotonic evolution of SC as CDW order is suppressed, Cr doping instead shows a slower suppression of CDW order and a rapid quenching of T_c. Given the strong disorder potential introduced by directly replacing the kagome net atoms, the impact of dopant-induced disorder remains uncertain in interpreting these phase diagrams. Naively, a cleaner means of introducing holes has been demonstrated via the substitution of Sn onto the Sb sites of $CsV_3Sb_{5-x}Sn_x$ which preserves the core V-based kagome matrix (Oey et al., 2022b). This doping away from the V-sites generates an anomalous double-dome evolution in T_c as long-range CDW order is destabilized. The electron-doping counterpart to this can be achieved via Te substitution onto the Sb sites in $CsV_3Sb_{5-x}Te_x$, which is the focus of this paper.

Here, we present x-ray diffraction, nuclear quadrupole resonance, and susceptibility measurements characterizing the Te-substituted (electron-doped) phase diagram of CsV_3Sb_5. Our data demonstrate a limited solubility of Te into the $CsV_3Sb_{5-x}Te_x$ matrix before phase separation occurs near $x \approx 0.08$ and that Te preferentially occupies the Sb sites in the V-kagome plane. In contrast to hole doping, the introduction of electrons results in a relatively weak perturbation to the system—where the CDW onset temperature is only slightly suppressed and SC is weakly suppressed in a monotonic fashion. The likely dominant driver of the weak suppression of both states is the introduction of disorder via Sb substitution, establishing a sharp contrast to the hole-doped phase diagram of this system.

2 Materials and methods

2.1 Powder and single crystal synthesis

Powders of $CsV_3Sb_{5-x}Te_x$ were synthesized inside a glovebox filled with argon (water and oxygen levels at < 0.5 ppm) by measuring stoichiometric amounts of elemental Cs (solid, Alfa 99.98%), V (powder, Sigma 99.9%, previously purified using a 1:10 ratio of EtOH and HCl), Sb (shot, Alfa 99.999%), and Te (lump, Alfa 99.999%). For each composition of Te doping, 6 g batches of the starting materials were ball-milled inside a tungsten carbide vial for 60 min in a SPEX 8000D high-energy ball mill. The resulting powders were extracted inside a glovebox, ground, and sieved through a 106 micron sieve. Powders were then placed inside an alumina crucible, sealed inside an argon-filled quartz tube, and annealed at 550°C for 48 h. A post-anneal grind and sieve was performed followed by a second anneal at 450°C for 12 h. The final powders are gray and reasonably air-stable.

Single crystals of $CsV_3Sb_{5-x}Te_x$ were grown by a self-flux method. Different Te concentrations were targeted by the formula $Cs_{20}V_{15}Sb_{120-x}Te_x$, with x = 7.2 and 9.6. Elements were weighed inside a glovebox to make 4 g batches of fluxes; each batch was loaded into tungsten carbide vials and ball-milled for 60 min. Precursors were then extracted, loaded into alumina crucibles, and sealed inside carbon-coated quartz tubes. Previous attempts at synthesizing $CsV_3Sb_{5-x}Te_x$ crystals were performed inside sealed steel tubes but were unsuccessful, given that elemental Te corrodes steel. The sealed tubes were heated at 900 °C for 12 h and then cooled to 500°C at 2°C/h. Single crystals were extracted manually using isopropyl alcohol.

2.2 Experimental details

Powder x-ray diffraction data were collected on a PANalytical Empyrean powder diffractometer. Pawley and Rietveld refinements were performed using *TOPAS-Academic* software (Coelho, 2018). A tabletop scanning tunneling microscope (SEM) (Hitachi TM4000Plus) was used to analyze concentrations of Te in single crystal samples. Magnetization data for both powders and crystals were measured inside a Quantum Design Magnetic Property Measurement System (MPMS) using the vibrating sample mode (VSM) to detect the superconducting transitions under a field of 5 Oe and measure the charge density wave transition under 10,000 Oe. Low-temperature susceptibility data were collected using a Quantum Design Physical Property Measurement System (PPMS) with a dilution refrigerator insert and the AC susceptibility option. Room-temperature ^{121}Sb zero-field nuclear quadrupole resonance (NQR) measurements were performed using a laboratory-made NMR spectrometer and probe. Quadrupole lines from the I = 5/2 Sb nuclei were collected from Fourier transforms of the spin-echo using the same sequence and approach as detailed in the work of Oey et al. (2022b). Two distinct Sb chemical sites are present in the unit cell, which we label Sb1 and Sb2, and they generate unique frequencies.

3 Results and discussion

Powders and single crystals of $CsV_3Sb_{5-x}Te_x$ were synthesized in the composition range $0 \leq x \leq 0.1$. The 300 K structure remains *P6/mmm* across this composition range, and the tellurium dopants occupy the Sb1 site in the kagome plane, as shown in Figure 1. Demonstrating this, NQR data plotted in Figure 1C, D show the preferential chemical shift of only the Sb2 sites at both NQR transitions probed. Using the same reasoning as that presented by Oey et al. (2022b), this indicates that Te preferentially occupies the in-plane Sb1 positions, as only changes to Sb1–Sb2 field gradients are observed and (similar distance) Sb2–Sb2 field gradients are unaffected.

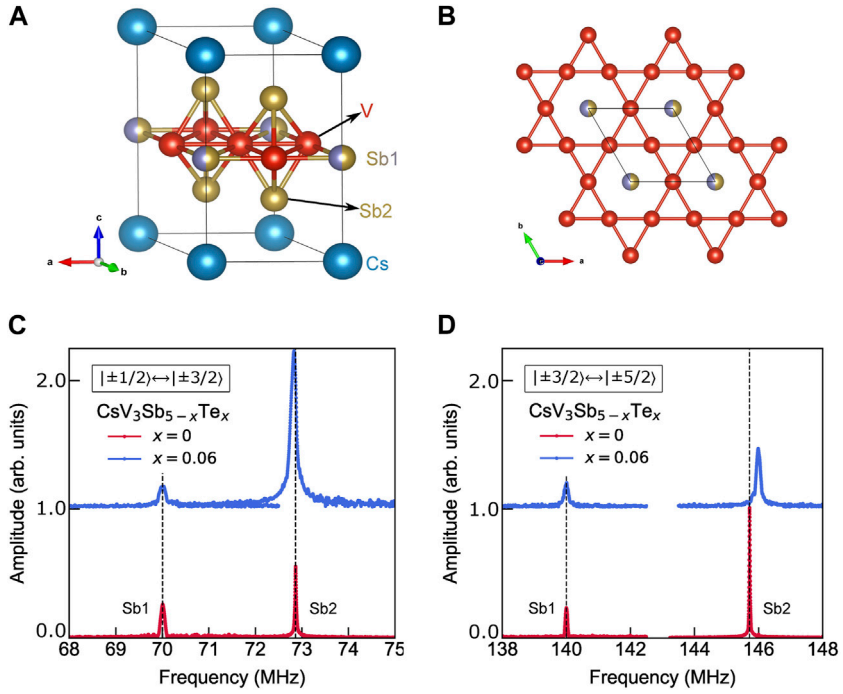

FIGURE 1
(A) Side and **(B)** top view of the $CsV_3Sb_{5-x}Te_x$ structure. NQR data are shown for the **(C)** first and **(D)** second transitions of the Sb1 and Sb2 sites, demonstrating that Te occupies the Sb1 site at $x = 0.06$.

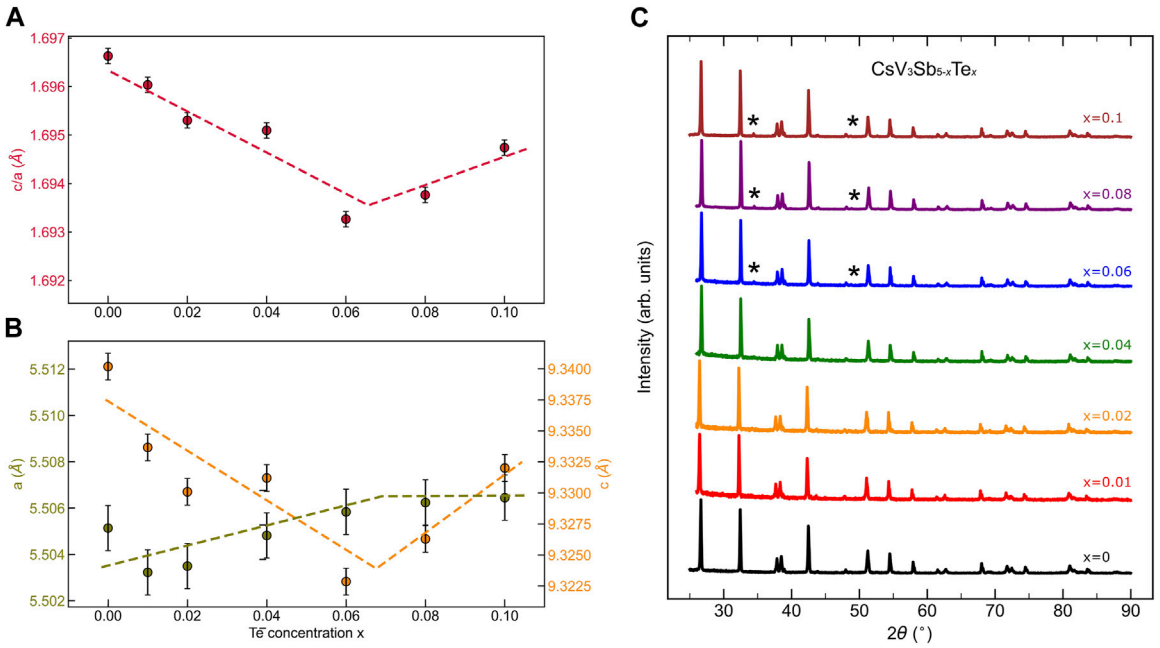

FIGURE 2
The $CsV_3Sb_{5-x}Te_x$ structure does not allow for significant chemical substitution beyond the $x = 0.1$ limit, at which a V-Sb impurity shows up. **(A)** Ratio of lattice parameters c/a as a function of x below this limit and **(B)** cell parameters a (left) and c (right) individually as a function of tellurium doping. **(C)** X-ray powder data collected for each concentration x with the onset of an impurity phase marked by * within the patterns. Numerical error bars from Pawley refinement are within the symbol size, and the larger error bars shown in **(A)** and **(B)** are estimated systematic errors.

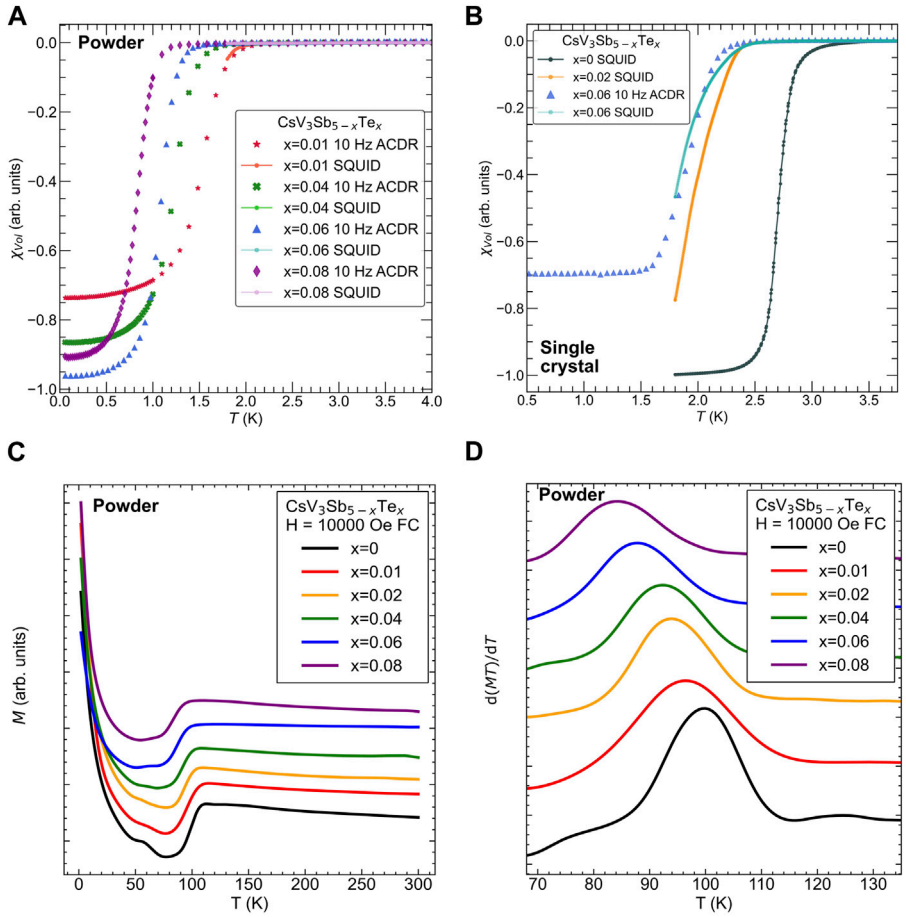

FIGURE 3
Superconducting transitions for $CsV_3Sb_{5-x}Te_x$ decrease with an increase in Te doping from the parent T_c at 2.5 K, as observed both in powder **(A)** and **(B)** crystal samples. Similarly, the charge density wave transition is weakly suppressed with electron doping, as revealed in **(C)**, showing the magnetization plotted as a function of temperature and more clearly in **(D)** in the plot of $d\,(MT)/d(T)$.

Lattice parameters derived from Pawley refinements of powder x-ray data are shown in Figure 2. The resulting *c/a* ratio plotted in Figure 2A reveals a continuous decrease up to a concentration of $x \approx 0.07$, and for concentrations greater than $x = 0.08$, impurity peaks are observed in the x-ray powder patterns, shown as '*' in Figure 2C. This suggests that the solubility limit is $x \approx 0.07$–0.08 of Te within the lattice, and a similar deviation from a linear Vergard-like behavior is suggested in the *a*- and *c*-axis lattice parameters plotted in Figure 2B on the left and right sides (although the changes are small and at the boundary of resolution).

Now turning to the characterization of $CsV_3Sb_{5-x}Te_x$ below the solubility limit, magnetization and susceptibility data are plotted in Figure 3. Figure 3A shows low-field susceptibility data characterizing the superconducting transition of polycrystalline $CsV_3Sb_{5-x}Te_x$ up to $x = 0.08$. Susceptibility data collected using a dilution insert (4 K–80 mK) was normalized to overlapping low-field magnetization-derived susceptibility data above 2 K. Within the uncertainty of this normalization procedure and variable packing fractions between powders, all specimens show a bulk superconducting transition in Figure 3A. In contrast to the effect of hole doping, T_c shows a monotonic and gradual decrease as a function of Te concentration.

Magnetization measurements collected under 10,000 Oe were performed at higher temperatures to characterize the CDW instability. These measurements can detect the onset of a CDW state via a decrease in the density of states at the Fermi level, reflected in a decrease in the Pauli spin susceptibility. Magnetization data plotted in Figure 3C reveal that a well-defined CDW transition remains observable for all compositions up to $x = 0.08$. This strongly contrasts the response observed upon hole doping, where the introduction of Sn immediately broadens and shifts the CDW transition. Quantifying the shift in the CDW onset temperature, Figure 3D plots the derivative $\delta MT/\delta T$, revealing a smooth shift downward in the CDW temperature upon Te doping with minimal broadening of the CDW anomaly in the magnetization data. This is again distinct from the response driven via hole substitution, where a rapid broadening immediately onsets and the CDW transition vanishes near $x = 0.05$ holes per formula unit. We note here that an upturn in the susceptibility at lower temperatures is also observed in all samples, and this can be modeled by a small fraction of paramagnetic ions in the powders (≈0.1% S = 1/2 moment per vanadium ion).

Our results are summarized in Figure 4, where the electronic phase diagram of hole- versus electron-doped CsV_3Sb_5 is plotted (i.e., Sn *versus* Te doped). Both electron and hole dopants result in the suppression of the CDW transition temperature; however, the suppression is more rapid for hole doping, and the transition vanishes near $x = 0.05$. In contrast, the suppression of the CDW temperature is more gradual with electron

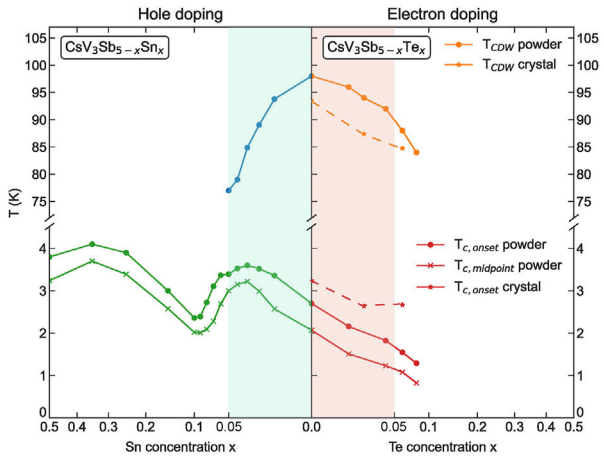

FIGURE 4
Plot of the electron–hole asymmetry in the electronic phase diagram of CsV_3Sb_5. Electron doping on the Sb site of CsV_3Sb_5 shows only a weak suppression of the CDW state, and the CDW state in the $CsV_3Sb_{5-x}Te_x$ system persists beyond Te = 0.05. The superconducting transition is only weakly suppressed under light electron doping in $CsV_3Sb_{5-x}Te_x$. This contrasts the dramatic suppression of the CDW order and the double-dome evolution of superconductivity that emerges upon hole doping. Data for hole doping via Sn substitution were adapted from the work of Oey et al. (2022b).

doping, and crucially, the CDW transition remains well defined until the solubility limit of Te is reached. The SC transition evolves smoothly downward with electron doping and does not follow a trivial enhancement via a trade-off in the density of states as the parent CDW state is weakened. This simultaneous suppression of the CDW onset temperature and T_c suggests that disorder introduced via chemical alloying may play a role in the suppression of each phase.

To test this, select single crystals of $CsV_3Sb_{5-x}Te_x$ were measured, and their transition temperatures were overplotted with those from powder samples in Figure 4. The apparent onset temperature of the CDW state is always higher in powders than in crystals, but both crystals and powders show a qualitatively similar smooth decrease in the CDW transition up to the solubility limit. However, the superconducting T_c in powders is often degraded relative to single crystals due to disorder effects (such as strain and plastic deformation) incurred during powder preparation. As a result, trends in T_c as a function of doping are often more reliable in crystals. Figure 4 shows that the T_c for single crystals of $CsV_3Sb_{5-x}Te_x$ is indeed higher than that of powders and that the suppression of T_c with Te doping is severely reduced. This supports the notion of a disorder-induced suppression of T_c as a function of impurity concentration rather than electron doping. Notably, the canonical trade-off between the suppressed CDW order and enhanced SC due to density of states effects is absent, further supporting the idea of a dominant role of the dopant-induced disorder.

The aforementioned results are derived using chemical dopants that avoid the V-sites in the kagome network; however, qualitatively similar trends in the evolution of CDW and SC order parameters have been reported in individual studies leveraging V-site substitution. Ti-doped CsV_3Sb_5 renders a phase diagram qualitatively similar to Sn-doped CsV_3Sb_5 (Yang et al., 2022), and Cr-doped CsV_3Sb_5 also reveals an asymmetric persistence of the CDW order (Ding et al., 2022). We note one difference: T_c is reported to be rapidly suppressed in Cr-doped samples, which is distinct from our Te-doped data. This is likely due to a stronger impurity potential native to the Cr dopants residing directly within the kagome network, and we hypothesize that the slow, simultaneous suppression of the CDW and SC is primarily driven by the dopant disorder.

4 Conclusion

In conclusion, our results illustrate a strong electron–hole asymmetry in the electronic phase diagram of carrier-doped CsV_3Sb_5. Electron doping via Te substitution in $CsV_3Sb_{5-x}Te_x$ largely preserves the CDW state, whereas hole doping rapidly suppresses the long-range CDW order and renormalizes the nature of charge correlations. At lower temperatures, light electron doping also largely preserves the superconducting state, whereas hole doping creates a non-monotonic, “double-dome” response. We suggest that the slight suppression in the onset temperatures of both the CDW and SC orders observed upon Te substitution arises from alloy-induced disorder rather than a doping-driven effect and that both transitions are robust to light electron doping. Our findings motivate a deeper theoretical exploration of electron–hole asymmetries in the carrier-tuned band structure of CsV_3Sb_5 and related compounds as a means of isolating the dominant Van Hove points and other band features responsible for driving electronic order in this family of compounds.

Data availability statement

The raw data supporting the conclusion of this article will be made available by the authors, without undue reservation.

Author contributions

AC: formal analysis, writing–original draft, and investigation. BO: formal analysis, investigation, and writing–review and editing. CB: formal analysis, investigation, and writing–review and editing. JF: formal analysis, investigation, and writing–review and editing. VM: formal analysis, writing–review and editing, resources, and supervision. SW: formal analysis, resources, supervision, conceptualization, funding acquisition, and writing–original draft.

Funding

The authors declare that financial support was received for the research, authorship, and/or publication of this article. SW, AC, and BO acknowledge support via the UC Santa Barbara NSF Quantum Foundry funded via the Q-AMASE-i program under award DMR-1906325. AC and BO acknowledge use of the shared experimental facilities of the NSF Materials Research Science and Engineering Center at UC Santa Barbara (DMR-1720256). The UC Santa Barbara MRSEC is a member of the Materials Research Facilities

Network (www.mrfn.org). This work was supported in part by the U.S. National Science Foundation (NSF) grant No. DMR-1905532 (VM). Work by BO was also supported by the U.S. Department of Energy (DOE), Office of Science, Basic Energy Sciences (BES), Materials Sciences and Engineering Division.

Conflict of interest

The authors declare that the research was conducted in the absence of any commercial or financial relationships that could be construed as a potential conflict of interest.

The author SW declares being an editorial board member of Frontiers at the time of submission. This had no impact on the peer review process and the final decision.

Publisher's note

All claims expressed in this article are solely those of the authors and do not necessarily represent those of their affiliated organizations, or those of the publisher, the editors, and the reviewers. Any product that may be evaluated in this article, or claim that may be made by its manufacturer, is not guaranteed or endorsed by the publisher.

References

Chen, K. Y., Wang, N. N., Yin, Q. W., Gu, Y. H., Jiang, K., Tu, Z. J., et al. (2021a). Double superconducting dome and triple enhancement of T_c in the kagome superconductor CsV_3Sb_5 under high pressure. *Phys. Rev. Lett.* 126, 247001. Publisher: American Physical Society. doi:10.1103/physrevlett.126.247001

Chen, X., Zhan, X., Wang, X., Deng, J., Liu, X.-B., Chen, X., et al. (2021b). Highly robust reentrant superconductivity in CsV_3Sb_5 under pressure. *Chin. Phys. Lett.* 38, 057402. Publisher: Chinese Physical Society and IOP Publishing Ltd. doi:10.1088/0256-307x/38/5/057402

Coelho, A. A. (2018). *TOPAS* and *TOPAS-Academic*: an optimization program integrating computer algebra and crystallographic objects written in C++. *J. Appl. Crystallogr.* 51, 210–218. doi:10.1107/S1600576718000183

Ding, G., Wo, H., Gu, Y., Gu, Y., and Zhao, J. (2022). Effect of chromium doping on superconductivity and charge density wave order in the kagome metal $Cs(V_{1-x}Cr_x)_3Sb_5$. *Phys. Rev. B* 106, 235151. Publisher: American Physical Society. doi:10.1103/physrevb.106.235151

Du, F., Li, R., Luo, S., Gong, Y., Li, Y., Jiang, S., et al. (2022). Superconductivity modulated by structural phase transitions in pressurized vanadium-based kagome metals. *Phys. Rev. B* 106, 024516. Publisher: American Physical Society. doi:10.1103/physrevb.106.024516

Du, F., Luo, S., Ortiz, B. R., Chen, Y., Duan, W., Zhang, D., et al. (2021). Pressure-induced double superconducting domes and charge instability in the kagome metal KV_3Sb_5. *Phys. Rev. B* 103, L220504. Publisher: American Physical Society. doi:10.1103/physrevb.103.l220504

Feng, X. Y., Zhao, Z., Luo, J., Yang, J., Fang, A. F., Yang, H. T., et al. (2023). Commensurateto-incommensurate transition of charge-density-wave order and a possible quantum critical point in pressurized kagome metal CsV3Sb5. *npj Quantum Mater* 8, 23–27. Number: 1 Publisher: Nature Publishing Group. doi:10.1038/s41535-023-00555-w

Hu, Y., Wu, X., Ortiz, B. R., Ju, S., Han, X., Ma, J., et al. (2022). Rich nature of van hove singularities in kagome superconductor CsV_3Sb_5. *Nat. Commun.* 13, 2220. doi:10.1038/s41467-022-29828-x

Kang, M., Fang, S., Kim, J.-K., Ortiz, B. R., Ryu, S. H., Kim, J., et al. (2022). Twofold van hove singularity and origin of charge order in topological kagome superconductor CsV_3Sb_5. *Nat. Phys.* 18, 301–308. doi:10.1038/s41567-021-01451-5

Kautzsch, L., Oey, Y. M., Li, H., Ren, Z., Ortiz, B. R., Seshadri, R., et al. (2022). *Incommensurate charge-stripe correlations in the kagome superconductor $CsV_3Sb_{5-x}Sn_x$*. ArXiv:2207.10608[cond-mat]. Available at: https://arxiv.org/abs/2207.10608 (Accessed July 21, 2022).

Kiesel, M. L., Platt, C., and Thomale, R. (2013). Unconventional fermi surface instabilities in the kagome hubbard model. *Phys. Rev. Lett.* 110, 126405. doi:10.1103/physrevlett.110.126405

LaBollita, H., and Botana, A. S. (2021). Tuning the van hove singularities in AV_3Sb_5 (A = K, Rb, Cs) via pressure and doping. *Phys. Rev. B* 104, 205129. Publisher: American Physical Society. doi:10.1103/physrevb.104.205129

Li, H., Zhang, T., Yilmaz, T., Pai, Y., Marvinney, C., Said, A., et al. (2021). Observation of unconventional charge density wave without acoustic phonon anomaly in kagome superconductors AV_3Sb_5 (A= Rb, Cs). *Phys. Rev. X* 11, 031050. doi:10.1103/physrevx.11.031050

Li, Y., Li, Q., Fan, X., Liu, J., Feng, Q., Liu, M., et al. (2022). Tuning the competition between superconductivity and charge order in the kagome superconductor $Cs(V_{1-x}Nb_x)_3Sb_5$. *Phys. Rev. B* 105, L180507. doi:10.1103/physrevb.105.l180507

Liu, M., Han, T., Hu, X., Tu, Y., Zhang, Z., Long, M., et al. (2022a). Evolution of superconductivity and charge density wave through Ta and Mo doping in CsV_3Sb_5. *Phys. Rev. B* 106, L140501. doi:10.1103/physrevb.106.l140501

Liu, Y., Liu, C.-C., Zhu, Q.-Q., Ji, L.-W., Wu, S.-Q., Sun, Y.-L., et al. (2022b). Enhancement of superconductivity and suppression of charge-density wave in As-doped CsV_3Sb_5. *Phys. Rev. Mater.* 6, 124803. Publisher: American Physical Society. doi:10.1103/physrevmaterials.6.124803

Liu, Y., Wang, Y., Cai, Y., Hao, Z., Ma, X.-M., Wang, L., et al. (2023). Doping evolution of superconductivity, charge order, and band topology in hole-doped topological kagome superconductors $Cs(V_{1-x}Ti_x)_3Sb_5$. *Phys. Rev. Mater.* 7, 064801. Publisher: American Physical Society. doi:10.1103/physrevmaterials.7.064801

Oey, Y. M., Kaboudvand, F., Ortiz, B. R., Seshadri, R., and Wilson, S. D. (2022a). Tuning charge density wave order and superconductivity in the kagome metals $KV_3Sb_{5-x}Sn_x$ and $RbV_3Sb_{5-x}Sn_x$. *Phys. Rev. Mater.* 6, 074802. doi:10.1103/physrevmaterials.6.074802

Oey, Y. M., Ortiz, B. R., Kaboudvand, F., Frassineti, J., Garcia, E., Cong, R., et al. (2022b). Fermi level tuning and double-dome superconductivity in the kagome metal $CsV_3Sb_{5-x}Sn_x$. *Phys. Rev. Mater.* 6, L041801. Publisher: American Physical Society. doi:10.1103/physrevmaterials.6.l041801

Ortiz, B. R., Capa Salinas, A. N., Knudtson, M. J., Sarte, P. M., Pokahrel, G., and Wilson, S. D. (2023). Complete miscibility amongst the AV_3Sb_5 kagome superconductors: design of mixed av_3sb_5 (a: k, rb, cs) alloys. *Phys. Rev. Mater.* 7, 014801. Publisher: American Physical Society. doi:10.1103/physrevmaterials.7.014801

Ortiz, B. R., Gomes, L. C., Morey, J. R., Winiarski, M., Bordelon, M., Mangum, J. S., et al. (2019). New kagome prototype materials: discovery of KV_3Sb_5, RbV_3Sb_5, and CsV_3Sb_5. *Phys. Rev. Mater.* 3, 094407. doi:10.1103/physrevmaterials.3.094407

Ortiz, B. R., Sarte, P. M., Kenney, E. M., Graf, M. J., Teicher, S. M., Seshadri, R., et al. (2021). Superconductivity in the Z2 kagome metal KV_3Sb_5. *Phys. Rev. Mater.* 5, 034801. doi:10.1103/physrevmaterials.5.034801

Ortiz, B. R., Teicher, S. M., Hu, Y., Zuo, J. L., Sarte, P. M., Schueller, E. C., et al. (2020). CsV_3Sb_5: a Z2 topological kagome metal with a superconducting ground state. *Phys. Rev. Lett.* 125, 247002. doi:10.1103/physrevlett.125.247002

Qian, T., Christensen, M. H., Hu, C., Saha, A., Andersen, B. M., Fernandes, R. M., et al. (2021). Revealing the competition between charge density wave and superconductivity in CsV_3Sb_5 through uniaxial strain. *Phys. Rev. B* 104, 144506. Publisher: American Physical Society. doi:10.1103/physrevb.104.144506

Song, B., Ying, T., Wu, X., Xia, W., Yin, Q., Zhang, Q., et al. (2023). Anomalous enhancement of charge density wave in kagome superconductor CsV_3Sb_5 approaching the 2D limit. *Nat. Commun.* 14, 2492. Number: 1 Publisher: Nature Publishing Group. doi:10.1038/s41467-023-38257-3

Song, Y., Ying, T., Chen, X., Han, X., Wu, X., Schnyder, A. P., et al. (2021). Competition of superconductivity and charge density wave in selective oxidized CsV_3Sb_5 thin flakes. *Phys. Rev. Lett.* 127, 237001. Publisher: American Physical Society. doi:10.1103/physrevlett.127.237001

Sur, Y., Kim, K.-T., Kim, S., and Kim, K. H. (2023). Optimized superconductivity in the vicinity of a nematic quantum critical point in the kagome superconductor $Cs(V_{1-x}Ti_x)_3Sb_5$. *Nat. Commun.* 14, 3899. Number: 1 Publisher: Nature Publishing Group. doi:10.1038/s41467-023-39495-1

Tan, H., Liu, Y., Wang, Z., and Yan, B. (2021). Charge density waves and electronic properties of superconducting kagome metals. *Phys. Rev. Lett.* 127, 046401. doi:10.1103/physrevlett.127.046401

Wang, N. N., Chen, K. Y., Yin, Q. W., Ma, Y. N. N., Pan, B. Y., Yang, X., et al. (2021a). Competition between charge-density-wave and superconductivity in the kagome metal RbV_3Sb_5. *Phys. Rev. Res.* 3, 043018. Publisher: American Physical Society. doi:10.1103/physrevresearch.3.043018

Wang, Q., Kong, P., Shi, W., Pei, C., Wen, C., Gao, L., et al. (2021b). Charge density wave orders and enhanced superconductivity under pressure in the kagome metal CsV_3Sb_5. *Adv. Mater.* 33, 2102813. doi:10.1002/adma.202102813

Wang, T., Yu, A., Zhang, H., Liu, Y., Li, W., Peng, W., et al. (2021c). *Enhancement of the superconductivity and quantum metallic state in the thin film of superconducting kagome metal KV_3Sb_5*. ArXiv:2105.07732 [cond-mat]. Available at: https://arxiv.org/abs/2105.07732 (Accessed May 17, 2021).

Wang, W.-S., Li, Z.-Z., Xiang, Y.-Y., and Wang, Q.-H. (2013). Competing electronic orders on kagome lattices at van hove filling. *Phys. Rev. B* 87, 115135. doi:10.1103/physrevb.87.115135

Xie, Y., Li, Y., Bourges, P., Ivanov, A., Ye, Z., Yin, J.-X., et al. (2022). Electron-phonon coupling in the charge density wave state of CsV_3Sb_5. *Phys. Rev. B* 105, L140501. doi:10.1103/physrevb.105.l140501

Yang, H., Huang, Z., Zhang, Y., Zhao, Z., Shi, J., Luo, H., et al. (2022). Titanium doped kagome superconductor $CsV_{3-x}Ti_xSb_5$ and two distinct phases. *Sci. Bull.* 67, 2176–2185. doi:10.1016/j.scib.2022.10.015

Yin, Q., Tu, Z., Gong, C., Fu, Y., Yan, S., and Lei, H. (2021). Superconductivity and normal-state properties of kagome metal RbV_3Sb_5 single crystals. *Chin. Phys. Lett.* 38, 037403. doi:10.1088/0256-307x/38/3/037403

Yu, F. H., Ma, D. H., Zhuo, W. Z., Liu, S. Q., Wen, X. K., Lei, B., et al. (2021). Unusual competition of superconductivity and charge-density-wave state in a compressed topological kagome metal. *Nat. Commun.* 12, 3645. Number: 1 Publisher: Nature Publishing Group. doi:10.1038/s41467-021-23928-w

Yu, F., Zhu, X., Wen, X., Gui, Z., Li, Z., Han, Y., et al. (2022). Pressure-induced dimensional crossover in a kagome superconductor. *Phys. Rev. Lett.* 128, 077001. Publisher: American Physical Society. doi:10.1103/physrevlett.128.077001

Zhang, Z., Chen, Z., Zhou, Y., Yuan, Y., Wang, S., Wang, J., et al. (2021). Pressure-induced reemergence of superconductivity in the topological kagome metal CsV_3Sb_5. *Phys. Rev. B* 103, 224513. Publisher: American Physical Society. doi:10.1103/physrevb.103.224513

Zheng, L., Wu, Z., Yang, Y., Nie, L., Shan, M., Sun, K., et al. (2022). Emergent charge order in pressurized kagome superconductor CsV_3Sb_5. *Nature* 611, 682–687. Number: 7937 Publisher: Nature Publishing Group. doi:10.1038/s41586-022-05351-3

Zhou, X., Li, Y., Liu, Z., Hao, J., Dai, Y., Wang, Z., et al. (2023). Effects of niobium doping on the charge density wave and electronic correlations in the kagome metal $Cs(V_{1-x}Nb_x)_3Sb_5$. *Phys. Rev. B* 107, 125124. Publisher: American Physical Society. doi:10.1103/physrevb.107.125124

Zhu, C. C., Yang, X. F., Xia, W., Yin, Q. W., Wang, L. S., Zhao, C. C., et al. (2022). Double-dome superconductivity under pressure in the V-based kagome metals AV_3Sb_5 (*A*: rb, k). *Phys. Rev. B* 105, 094507. Publisher: American Physical Society. doi:10.1103/physrevb.105.094507